Procedia Computer Science

Volume 80, 2016, Pages 1324–1333

ICCS 2016. The International Conference on Computational Science

A Two-Scale Reduced Model for Darcy Flow in Fractured Porous Media

Huangxin Chen[1] and Shuyu Sun[2]

[1] School of Mathematical Sciences and Fujian Provincial Key Laboratory on Mathematical Modeling and High Performance Scientific Computing, Xiamen University, Fujian, 361005, China, and King Abdullah University of Science and Technology (KAUST), Physical Science and Engineering Division (PSE), Thuwal, 23955-6900, Saudi Arabia.
chx@xmu.edu.cn

[2] King Abdullah University of Science and Technology (KAUST), Physical Science and Engineering Division (PSE), Thuwal, 23955-6900, Saudi Arabia.
shuyu.sun@kaust.edu.sa

Abstract

In this paper, we develop a two-scale reduced model for simulating the Darcy flow in two-dimensional porous media with conductive fractures. We apply the approach motivated by the embedded fracture model (EFM) to simulate the flow on the coarse scale, and the effect of fractures on each coarse scale grid cell intersecting with fractures is represented by the discrete fracture model (DFM) on the fine scale. In the DFM used on the fine scale, the matrix-fracture system are resolved on unstructured grid which represents the fractures accurately, while in the EFM used on the coarse scale, the flux interaction between fractures and matrix are dealt with as a source term, and the matrix-fracture system can be resolved on structured grid. The Raviart-Thomas mixed finite element methods are used for the solution of the coupled flows in the matrix and the fractures on both fine and coarse scales. Numerical results are presented to demonstrate the efficiency of the proposed model for simulation of flow in fractured porous media.

Keywords: Fractured porous media, two-scale, discrete fracture model, embedded fracture model, mixed finite element method.

1 Introduction

Modeling flow in fractured porous media plays a significant role in many applications such as energy problems. The fractures representing strong heterogeneities are usually much permeable than that in the surrounding matrix, and the width of fracture may be much smaller than any reasonable mesh size for spatial discretization. One might utilize the single-domain model to tackle the problem, however this needs to refine the mesh locally around the fractures and

 Selection and peer-review under responsibility of the Scientific Programme Committee of ICCS 2016

doi:10.1016/j.procs.2016.05.417

results in very expensive computations. Various models which include dual porosity model, dual porosity dual permeability model, discrete fracture model (DFM) and some improvements have been studied during the past several decades; see, e.g.,[1, 16, 2, 6, 14, 9, 10, 15, 8] and the references therein.

In naturally fractured rock system with many fractures, a framework based on a number of overlapping continua may be established, e.g., dual porosity, dual permeability models. In order to obtain more accurate simulations, the DFM is proposed to deal with the fractures as lower dimensional surfaces in the computational domain [14, 9, 10]. We point out that in the DFM used in this paper, the interaction between the fractures and the surrounding matrix is considered so that refining locally around the fractures can be avoided. However, in this approach, the grid should be generated according to the geometry and locations of fractures such that the grid cell for fractures are located at the matrix cell interface. This can be done by using complex unstructured grid generation strategy but leads to a large system. In order to avoid generating complex conforming grid, one approach called the extended finite element method (XFEM) was applied in [7, 5] by enriching the finite element basis on the elements cut by the fractures with discontinuous functions, and the matrix grid and the fracture grid can be non-matching at the intersection. Another approach, the concept of the embedded fracture model (EFM) was introduced by Lee et al. [11, 12, 13]. In these works, the flow in fractured porous media is simulated by a hierarchical fracture modeling. The small scale fractures are homogenized, while the long fractures are treated as low dimensional objects and the flux interaction between fractures and matrix are dealt with as a source term. The EFM can avoid using complex grid for matrix-fracture system and may lead to a smaller system compared with the DFM. Some extensions and applications of the EFM in the multiscale approach were introduced in [8] for iterative multiscale finite volume method and in [4] for generalized multiscale finite element method.

In this paper, a two-scale reduced model is devised which combines the concepts of DFM and EFM. We assume that the permeability is homogeneous in the matrix. In the coarse scale, we apply the EFM for simulating the flow in fractured porous media to avoid using complex grid on the whole domain. The flux interaction between fractures and matrix is modeled in a volume V intersecting with a fracture γ as a volume averaged source in matrix and a face averaged source in fractures $T_V^{mf}d\boldsymbol{x} = \eta K_m(\overline{p}_\gamma - \overline{p}_m)/|V|$ and $T_\gamma^{fm} = \eta K_m(\overline{p}_m - \overline{p}_\gamma)/|\gamma|$, where K_m is permeability of the matrix, $\overline{p}_m$ is the volume average of matrix pressure, $\overline{p}_\gamma$ is the face average of fracture pressure and η is a grid dependent parameter which is related with the location of fracture in the volume V. In the literatures [11, 12, 13, 8], it is assumed that the matrix pressure around a fracture is linearly distributed in a grid-block, then the grid dependent parameter η deserves a detailed computation identity which will be discussed in the following section. However, in most real problems this assumption is not usually satisfied, for instance, the case when there are more than one fractures in the grid-block. Therefore, in order to obtain a more accurate grid dependent parameter in the EFM, we apply the DFM on fine scale to resolve the parameter on each coarse scale grid cell intersecting with fractures by oversampling technique in a larger sample domain which reduces the influence of setting of boundary conditions. On the coarse scale for the EFM, we utilize the Raviart-Thomas mixed finite element approximation of the lowest order (RT_0), the next order of which (RT_1) is used for the DFM on the fine scale.

The paper is organized as follows: In section 2, we introduce some notations, the DFM and the EFM for Darcy flow in fractured porous media. The two-scale reduced model and the associated Raviart-Thomas mixed finite element approximation is introduced in section 3. In section 4, we present some numerical experiments for simulations of the two-scale model for

flow in fractured porous media to verify the efficiency of the new model. Finally, the paper is concluded in section 5.

2 Preliminaries

In this paper, we consider the simulation of single-phase Darcy flow in the fractured porous media. Let $\Omega \in \mathbb{R}^2$ be a bounded and simply connected fractured porous media domain with Lipschitz continuous boundary. When the inertial effect is neglected, the single-phase flow in Ω governed by mass conservation and Darcy's law can be written as:

$$\nabla \cdot \boldsymbol{u} = q \qquad \text{in} \quad \Omega, \tag{2.1a}$$

$$\boldsymbol{u} = -\boldsymbol{K}\nabla p \qquad \text{in} \quad \Omega, \tag{2.1b}$$

where p is the pressure, $\boldsymbol{u}$ is the Darcy velocity, $\boldsymbol{K}$ is a bounded symmetric and positive definite permeability tensor, and q is the source term. We assume Dirichlet boundary condition and Neumann boundary condition are both imposed on parts of $\partial\Omega$. Since Ω is a fractured porous media, $\boldsymbol{K}$ is a heterogeneous permeability tensor which has high values in fractures and low values in matrix. To simulate (2.1) in the fractured porous media, we consider the DFM and the EFM approaches in the following.

2.1 Discrete fracture model

In order to introduce the DFM for simplicity, we assume that there is a single fracture subdomain in the porous media and the domain Ω is separated into three connected subdomains Ω_1, Ω_2 and Ω_f as shown in the left graph of Figure 1.

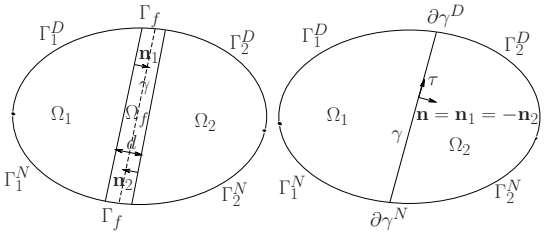

Figure 1: (For the DFM) Left: The domain Ω with a single fracture subdomain Ω_f. Right: The subdomains Ω_1, Ω_2 and the reduced fracture γ.

The matrix domain is denoted by $\Omega_m = \Omega_1 \cup \Omega_2$. The fracture domain Ω_f is assumed as $\Omega_f = \{x \in \Omega : x = s + t\boldsymbol{n},\ s \in \gamma \text{ and } t \in (-\frac{d(s)}{2}, \frac{d(s)}{2})\}$, where γ is a one-dimensional polygonal line, $\boldsymbol{n} = \boldsymbol{n}_1 = -\boldsymbol{n}_2$ is the unit normal vector to γ, $\boldsymbol{n}_i|_{i=1,2}$ is the unit normal on $\partial\Omega_i \cap \partial\Omega_f$ outwards with respect to Ω_i, and $d(s)$ denotes the thickness of fracture at the point $s \in \gamma$. Let $\boldsymbol{\tau}$ be the unit tangential vector to γ. The permeability tensors in matrix and fracture are denoted by $\boldsymbol{K}_m = K_m\boldsymbol{I}$ and $\boldsymbol{K}_f = K_f\boldsymbol{I}$ respectively, where $K_f \gg K_m > 0$ and $\boldsymbol{I}$ is identity matrix. We will use the reduced model proposed in [14] based on the DFM which couples the interaction between the fractures and the surrounding matrix. We denote by $\nabla_{\boldsymbol{\tau}}$ and $\nabla_{\boldsymbol{\tau}}\cdot$ the tangential gradient and divergence operators along γ. Let $\boldsymbol{u}_i, p_i, q_i$ be the restrictions of $\boldsymbol{u}, p, q$ in Ω_i for $i = 1, 2, f$. We denote by $\{\cdot\}_\gamma$ the average of a quantity on γ such that $\{\psi\}_\gamma = \frac{1}{2}(\psi_1|_\gamma + \psi_2|_\gamma)$ and $[\![\cdot]\!]_\gamma$ the jump of a quantity across γ such that $[\![\psi]\!]_\gamma = \psi_1|_\gamma - \psi_2|_\gamma$, where $\psi_i|_{i=1,2}$ is a

function defined in Ω_i with well-defined trace on γ. The reduced model for flow within the domain in the right graph of Figure 1 is written as (cf. [14]):

$$\nabla \cdot \boldsymbol{u}_i = q_i \quad \text{in} \quad \Omega_i,\ i = 1, 2, \tag{2.2a}$$
$$\boldsymbol{u}_i = -\boldsymbol{K}_m \nabla p_i \quad \text{in} \quad \Omega_i,\ i = 1, 2, \tag{2.2b}$$

together with the reduced equations

$$\nabla_{\boldsymbol{\tau}} \cdot \boldsymbol{u}_\gamma = q_\gamma + [\![\boldsymbol{u} \cdot \boldsymbol{n}]\!]_\gamma \quad \text{on} \quad \gamma, \tag{2.2c}$$
$$\widehat{\eta}_\gamma \boldsymbol{u}_\gamma + \nabla_{\boldsymbol{\tau}} p_\gamma = 0 \quad \text{on} \quad \gamma, \tag{2.2d}$$

and the interface conditions

$$\xi_\gamma \eta_\gamma [\![\boldsymbol{u} \cdot \boldsymbol{n}]\!]_\gamma = \{p\}_\gamma - p_\gamma \quad \text{on} \quad \gamma, \tag{2.2e}$$
$$\eta_\gamma \{\boldsymbol{u} \cdot \boldsymbol{n}\}_\gamma = [\![p]\!]_\gamma, \quad \text{on} \quad \gamma, \tag{2.2f}$$

where $\boldsymbol{u}_\gamma = \int_{-\frac{d(s)}{2}}^{\frac{d(s)}{2}} (\boldsymbol{u}_f(s,t) \cdot \boldsymbol{\tau}(s)) \boldsymbol{\tau}(s) dt$, $p_\gamma = \frac{1}{d(s)} \int_{-\frac{d(s)}{2}}^{\frac{d(s)}{2}} p_f(s,t) dt$ and $q_\gamma = \int_{-\frac{d(s)}{2}}^{\frac{d(s)}{2}} q_f(s,t) dt$. Actually, the equations (2.2c-2.2d) are obtained by averaging the conservation equation (2.1a) and the Darcy's law (2.1b) over cross-section of the fracture Ω_f. The parameters in (2.2e) and (2.2f) are defined as $\widehat{\eta}_\gamma^{-1} = d(s) K_f$, $\eta_\gamma = d(s)/K_f$ and $\xi_\gamma = \frac{2\xi - 1}{4}$, $\xi > 1/2$. The above matrix-fracture reduced system can be solved combining Dirichlet or Neumann boundary conditions. Since the fractures are more permeable than that in the surrounding matrix, the Neumann boundary condition on $\partial\gamma^N$, which is immersed in the porous media, can be considered as $\boldsymbol{u}_\gamma \cdot \boldsymbol{\tau}|_{\partial\gamma^N} = 0$. The above reduced DFM (2.2) can be extended to the problem with more reduced non-intersecting fractures which are non-immersed, partially immersed or totally immersed in the porous media. For the problem with intersecting fractures, besides the interface conditions across the fractures mentioned in (2.2), the reduced model should also be coupled with additional coupling conditions at the intersection points for the fracture-fracture system [7, 5].

2.2 Embedded fracture model

In order to avoid using the complex conforming grid for the reduced DFM, the EFM (cf. [11, 12, 13]) was introduced by treating the long fractures as low dimensional objects and the flux interaction between fractures and matrix as a source term. Actually, the EFM can also be applied for shorter fractures. For the EFM simulating the flow in the matrix-fracture system as in Figure 2, we consider the governing equations in the matrix

$$\nabla \cdot \boldsymbol{u}_m = T^{mf} + q_m \quad \text{in} \quad \Omega_m, \tag{2.3a}$$
$$\boldsymbol{u}_m = -\boldsymbol{K}_m \nabla p_m \quad \text{in} \quad \Omega_m, \tag{2.3b}$$

together with the reduced equations in lower dimensional reduced fractures

$$\nabla_{\boldsymbol{\tau}} \cdot \boldsymbol{u}_\gamma = T^{fm} + q_\gamma \quad \text{on} \quad \gamma, \tag{2.3c}$$
$$\widehat{\eta}_\gamma \boldsymbol{u}_\gamma + \nabla_{\boldsymbol{\tau}} p_\gamma = 0 \quad \text{on} \quad \gamma, \tag{2.3d}$$

where T^{mf} and T^{fm} are the flux interactions between fractures and matrix. The governing equations used in fracture network in [11, 12, 13] are the same as that in the non-reduced fractures. Here, we use the similar reduced equations in the fracture network as in the DFM.

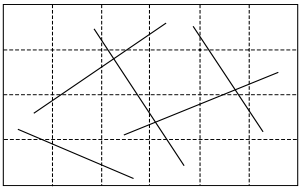

Figure 2: Two-dimensional matrix Ω_m with one-dimensional fracture network γ.

By the fact that the total flux balance between fractures and matrix should be guarantied in a volume V, we have $\int_V T^{mf} d\boldsymbol{x} + \int_{\gamma_v} T^{fm} d\boldsymbol{s} = 0$, where γ_v is the reduced fracture network containing in the volume V. When there is a single fracture γ_v in a volume V, the flux interaction can be modeled (cf. [13, 8]) as the face averaged source $T^{fm}_{\gamma_v} = \eta K_m(\overline{p}_m - \overline{p}_{\gamma_v})/|\gamma_v|$ in the discrete conservation law in the fracture and the volume averaged source $T^{mf}_V = \eta K_m(\overline{p}_{\gamma_v} - \overline{p}_m)/|V|$ in the discrete conservation law in the matrix. Here $T^{mf}_{\gamma_v}$ and T^{mf}_V are face average and volume average of the flux interaction T^{mf}. From the viewpoint of DFM, one can easily see that

$$\int_{\gamma_v} T^{fm} d\boldsymbol{s} = \int_{\gamma_v} [\![\boldsymbol{u}_m \cdot \boldsymbol{n}]\!]_{\gamma_v} d\boldsymbol{s} = K_m \int_{\gamma_v} [\![\nabla p_m \cdot \boldsymbol{n}]\!]_{\gamma_v} d\boldsymbol{s}.$$

When the matrix pressure around a fracture is assumed to be linearly distributed in the volume V, e.g., $p_m|_{\gamma_v} = 0, |\nabla p_m| = 1, \nabla p_m \perp \gamma_v$ and $p_m \geq 0$, then one can get $p_m = d_{\gamma_v}(\boldsymbol{x})$ where $d_{\gamma_v}(\boldsymbol{x})$ is the distance between a node $\boldsymbol{x} \in V$ and γ_v. When K_f is large enough, one can assume $p_{\gamma_v} = 0$ in this case and derive the identity for the grid dependent parameter as

$$\eta = 2|\gamma_v|/\langle d_{\gamma_v} \rangle, \tag{2.4}$$

where $\langle d_{\gamma_v} \rangle = \int_V d_{\gamma_v}(\boldsymbol{x}) d\boldsymbol{x}/|V|$.

The assumption of linear distributed matrix pressure around a fracture is usually used in the EFM [13, 8]). However, this assumption does not always hold true, i.e., the identity (2.4) for η is not always exactly satisfied. Therefore, in the next section we will consider two-scale model and compute more accurate estimate for the grid dependent parameter on the fine scale.

3 The two-scale model and mixed finite element approximation

In this section we consider a two-scale reduced model for simulating the flow in fractured porous media. In the following, we always assume the whole fractured porous media is a two-dimensional rectangular domain. On the coarse scale, we utilize the EFM based on the structured grid. As discussed in section 2.2, the grid dependent parameter relation (2.4) is not always exactly satisfied in a volume. We will consider oversampling technique and solve the local problems based on the DFM on a fine scale grid to recover this parameter on each fracture in a coarse scale grid cell.

Figure 3 shows the cases that the fractures non-immersed or partially immersed in the coarse scale grid cell T_c. There may be more complex fracture system in a coarse scale grid cell. If some parts of fractures locate at the face of coarse scale grid cells, the union of which will be used to compute the grid dependent parameter. The fracture in T_c is extended artificially

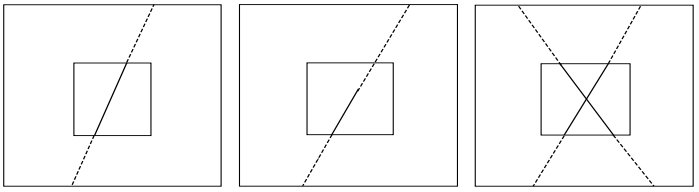

Figure 3: The extended domain used for the oversampling technique. The central rectangular subdomain in each graph denotes for the coarse scale grid cell T_c intersecting with fracture. Left: one fracture non-immersed in T_c. Middle: one fracture partially immersed in T_c. Right: Two intersecting fractures non-immersed in T_c.

to be a non-immersed fracture γ^E in the larger extended matrix domain Ω_m^E. The Dirichlet boundary conditions are imposed both for the equations in matrix and fractures in the reduced model (2.2), e.g., we let $p_m = 1$ on $\partial\Omega_m^E$ and $p_\gamma = 0$ on $\partial\gamma^E$. We assume there are $\gamma_1^E, \cdots, \gamma_N^E$ fractures in Ω_m^E. For each $\gamma_k = \gamma_k^E \cap T_c$, let

$$T_{\gamma_k}^{fm} = \frac{1}{|\gamma_k|}\int_{\gamma_k} [\![\boldsymbol{u}_m \cdot \boldsymbol{n}]\!]_{\gamma_k} d\boldsymbol{s} = \frac{\alpha}{h_T} K_m(\overline{p}_m - \overline{p}_{\gamma_k}), \tag{3.1}$$

where $h_T = |T_c|^{\frac{1}{2}}$, i.e., the grid dependent parameter η in the flux interaction at γ_k is determined by $\eta|_{\gamma_k} = \alpha|\gamma_k|/h_T$. Then the volume average of the flux interaction $T_{T_c}^{mf}$ can be correspondingly determined. Since the pressure changes slightly inside highly conductive fractures, the definition of α in (3.1) makes sense and will be used in the following as the grid dependent parameter.

One can refer to [14] for the weak formulation of (2.2) and the associated well-posedness property. We introduce the well-known Raviart-Thomas mixed finite element space of order k as: $\mathrm{RT}_k = [\mathbb{P}_k]^2 \oplus \boldsymbol{x}\mathbb{P}_k$, where $\mathbb{P}_k$ is the polynomial space of degree $k \geq 0$. In the numerical experiments, we use the RT_1 space for velocity and piecewise $\mathbb{P}_1$ space for pressure to solve (2.2). The fine scale grid used for the solution of (2.2) is conforming, unstructured and matched at the lower dimensional fractures. We can get the estimates for the grid dependent parameter α according to (3.1) after the numerical solution of (2.2) in the extended matrix-fracture system.

Now we consider the numerical solution of (2.3) on the coarse scale grid. We denote by Γ_m^N, Γ_m^D the Neumann and Dirichlet boundaries for the flow equations (2.3a-2.3b) in matrix and $\partial\gamma^D, \partial\gamma^N$ the Neumann and Dirichlet boundaries for the flow equations (2.3c-2.3d) in the lower dimensional fractures. Then the system (2.3) can be solved by combining the boundary conditions $\boldsymbol{u}_m \cdot \boldsymbol{n}_\Gamma|_{\Gamma_m^N} = g_m^N, p_m|_{\Gamma_m^D} = g_m^D, \boldsymbol{u}_\gamma \cdot \boldsymbol{\tau}|_{\partial\gamma^N} = g_\gamma^N, p_\gamma|_{\partial\gamma^N} = g_\gamma^D$, where $\boldsymbol{n}_\Gamma$ is the unit outward normal on $\partial\Omega_m$. Standard notations and definitions for Sobolev spaces are used throughout the paper. Let $\mathcal{T}_h^m$ be a conforming structured grid of Ω_m and $\mathcal{T}_h^\gamma$ be the finite element partition of lower dimensional fracture network γ. We use the same degrees of freedom for the fracture pressure at the intersection points of fractures. For simplicity, we assume $g_m^N \in \mathrm{P}_k(\Gamma_m^N)$, $g^N = (g_m^N, g_\gamma^N)$ and define the finite element spaces $\boldsymbol{U}_h^{g^N} = \boldsymbol{U}_{m,h}^{g_m^N} \times \boldsymbol{U}_{\gamma,h}^{g_\gamma^N}$ and $Q_h = Q_{m,h} \times Q_{\gamma,h}$, where

$$\boldsymbol{U}_{m,h}^{g_m^N} = \{\boldsymbol{v}_m \in H(\mathrm{div}, \Omega_m) : \boldsymbol{v}_m|_T \in \mathrm{RT}_k(T), \forall\, T \in \mathcal{T}_h^m; \boldsymbol{v}_m \cdot \boldsymbol{n}_\Gamma|_{\Gamma_m^N} = g_m^N\},$$

$$Q_{m,h} = \{r_m \in L^2(\Omega_m) : \ r_m|_T \in \mathbb{P}_k(T), \ \forall\, T \in \mathcal{T}_h^m\},$$

and

$$\boldsymbol{U}_{\gamma,h}^{g_\gamma^N} = \{\boldsymbol{v}_\gamma \in H(\mathrm{div}_{\boldsymbol{\tau}}, \gamma) : \boldsymbol{v}_\gamma|_e \in \mathrm{RT}_k(e), \forall\, e \in \mathcal{T}_h^\gamma; \boldsymbol{v}_\gamma \cdot \boldsymbol{\tau}|_{\Gamma_\gamma^N} = g_\gamma^N\},$$

$$Q_{\gamma,h} = \{r_\gamma \in L^2(\gamma) : \ r_\gamma|_e \in \mathbb{P}_k(e), \ \forall\, e \in \mathcal{T}_h^\gamma\}.$$

For any functions $\boldsymbol{v}_h^* \in \boldsymbol{U}_h^{g^N}$ and $r_h^* \in Q_h$, we denote $\boldsymbol{v}_h^* = (\boldsymbol{v}_{m,h}, \boldsymbol{v}_{\gamma,h})$ and $r_h^* = (r_{m,h}, r_{\gamma,h})$. For any $e \in \mathcal{T}_h^\gamma$, we denote by $\mathcal{E}_e = \{e' : e' = e \cap T, T \in \mathcal{T}_h^m\}$. If $e \subset T, T \in \mathcal{T}_h^m$, then $\mathcal{E}_e = e$. Let $(T^{mf}, r_{m,h})_{\Omega_m}$ and $(T^{fm}, r_{\gamma,h})_\gamma$ be defined as follows:

$$(T^{mf}, r_{m,h})_{\Omega_m} = \sum_{e \in \mathcal{T}_h^\gamma} \sum_{\substack{e' \in \mathcal{E}_e \\ e' \subset T \in \mathcal{T}_h^m}} \frac{\alpha_{e'}|e'|}{h_T} K_m (p_{\gamma,h}^{e'} - p_{m,h}^T) r_{m,h}^T,$$

$$(T^{fm}, r_{\gamma,h})_\gamma = \sum_{e \in \mathcal{T}_h^\gamma} \sum_{\substack{e' \in \mathcal{E}_e \\ e' \subset T \in \mathcal{T}_h^m}} \frac{\alpha_{e'}|e'|}{h_T} K_m (p_{m,h}^T - p_{\gamma,h}^{e'}) r_{\gamma,h}^{e'}.$$

Here $\alpha_{e'}$ is the grid dependent parameter α in (3.1) limited on $e' \in \mathcal{E}_e, e \in \mathcal{T}_h^\gamma$, $r_{m,h}^T$ and $r_{\gamma,h}^{e'}$ are the volume average of $r_{m,h}$ on T and the face average of $r_{\gamma,h}$ on e'. Let $Q_h^T = \{r \in L^2(\Omega_m) : r|_T \in \mathrm{P}_0(T), T \in \mathcal{T}_h^m\}$ and $Q_h^E = \{r \in L^2(\gamma) : r|_{e'} \in \mathrm{P}_0(e'), e' \in \mathcal{E}_e, e \in \mathcal{T}_h^\gamma\}$. The discrete weak formulation of (2.3) can be written as: Find $(\boldsymbol{u}_h^*, p_h^*) \in \boldsymbol{U}_h^{g^N} \times Q_h$ and $(p_{m,h}^T, p_{\gamma,h}^{e'}) \in Q_h^T \times Q_h^E$ such that

$$a(\boldsymbol{u}_h^*, \boldsymbol{v}_h^*) - b(\boldsymbol{v}_h^*, p_h^*) = G(g^D, \boldsymbol{v}_h^*) \qquad \forall\, \boldsymbol{v}_h^* \in \boldsymbol{U}_h^0, \tag{3.2a}$$

$$b(\boldsymbol{u}_h^*, r_h^*) + c(p_h^*, r_h^*) = L(q^*, r_h^*) \qquad \forall\, r_h^* \in Q_h, \tag{3.2b}$$

$$(p_{m,h}, 1)_T/|T| = p_{m,h}^T, \qquad \forall\, T \in \mathcal{T}_h^m, \tag{3.2c}$$

$$(p_{\gamma,h}, 1)_{e'}/|e'| = p_{\gamma,h}^{e'}, \qquad \forall\, e' \in \mathcal{E}_e, e \in \mathcal{T}_h^\gamma, \tag{3.2d}$$

where

$$\begin{aligned}
a(\boldsymbol{u}_h^*, \boldsymbol{v}_h^*) &= (\boldsymbol{K}_m^{-1} \boldsymbol{u}_{m,h}, \boldsymbol{v}_{m,h})_{\Omega_m} + (\widehat{\eta}_\gamma \boldsymbol{u}_{\gamma,h}, \boldsymbol{v}_{\gamma,h})_\gamma, \\
b(\boldsymbol{u}_h^*, r_h^*) &= (\nabla \cdot \boldsymbol{u}_{m,h}, r_{m,h})_{\Omega_m} + (\nabla_{\boldsymbol{\tau}} \cdot \boldsymbol{u}_{\gamma,h}, r_{\gamma,h})_\gamma, \\
c(p_h^*, r_h^*) &= -(T^{mf}, r_{m,h})_{\Omega_m} - (T^{fm}, r_{\gamma,h})_\gamma, \\
G(g^D, \boldsymbol{v}^*) &= -\left(g_m^D, \boldsymbol{v}_{m,h} \cdot \boldsymbol{n}_\Gamma\right)_{\Gamma_m^D} - \left(g_\gamma^D, \boldsymbol{v}_{\gamma,h} \cdot \boldsymbol{n}_\Gamma\right)_{\partial\gamma^D}, \\
L(q^*, r^*) &= (q_m, r_m)_{\Omega_m} + (q_\gamma, r_{\gamma,h})_\gamma.
\end{aligned}$$

Obviously, when we utilize the lowest order of Raviart-Thomas mixed finite element approximation, the system (3.2) will reduce to find $(\boldsymbol{u}_h^*, p_h^*) \in \boldsymbol{U}_h^{g^N} \times Q_h$ satisfying (3.2a-3.2b). One can refer to [3, Chapter II] for the well-posedness of this discrete weak formulation.

4 Numerical experiments

In this section, we will present several numerical experiments to show the efficiency of the two-scale reduced model for Darcy flow in fractured porous media. We assume the thickness of fracture is always 0.01 in the experiments. When the reduced DFM (2.2) is applied, the parameter ξ_γ in (2.2e) is chosen as $\xi_\gamma = 1/8$. The source terms q_m and q_γ in (2.2) and (2.3) are both set to be zeros in the following experiments.

The flux interaction identity (3.1) is used in the EFM in highly conductive fractures. Firstly, we show the relationship between the grid dependent parameter α in (3.1) and K_f/K_m when

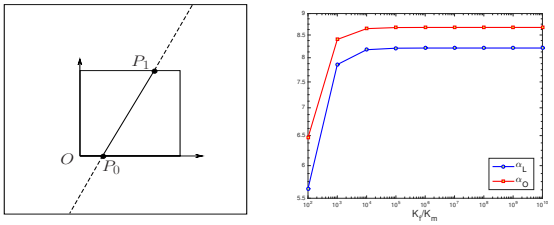

Figure 4: Left: The extended domain used for the oversampling technique. Right: Relationship between the grid dependent parameter α in (3.1) and K_f/K_m.

the position of a single fracture in a grid cell is fixed. As shown in left graph of Figure 4, we consider a single fracture in a unit square domain $\Omega_c = [0,1] \times [0,1]$. The two ends of the fracture are set to be $P_0 = (0.2, 0)$ and $P_1 = (0.8, 1)$. The reference domain Ω_c is extended to a larger domain $\Omega^E = [-1,2] \times [-1,2]$, and the fracture is also extended to be non-immersed in Ω^E. We denote by α_L the grid dependent parameter α obtained based on linear boundary condition, and α_O the grid dependent parameter α obtained by oversampling technique based on the DFM in domain Ω^E. From the right graph of Figure 4, we can see that both α_L and α_O are almost a fixed constant when K_f/K_m is large enough. For other cases of single fracture in Ω_c, the same property can also be observed. Generally, one can compute a series of α based on a sample of different locations of fractures in Ω_c, and obtain the approximate α for other location of fracture by interpolation technique.

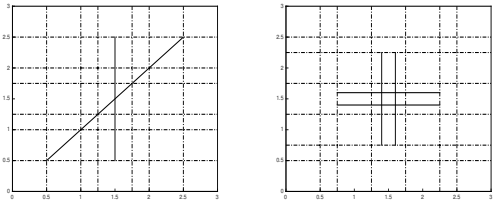

Figure 5: Case 1 (left): A domain with two intersecting fractures; Case 2 (right): A domain with four intersecting fractures.

Table 1: The errors $E^p_{m,H}$ and $E^p_{\gamma,H}$ for different choices of α.

Case 1	$E^p_{m,H}$	3.9851e-2 (α_L)	3.7956e-2 (α_O)	3.8118e-2 (α^*_O)
	$E^p_{\gamma,H}$	2.0780e-5 (α_L)	1.9415e-5 (α_O)	1.9862e-5 (α^*_O)
Case 2	$E^p_{m,H}$	4.9533e-2 (α_L)	4.7542e-2 (α_O)	3.9145e-2 (α^*_O)
	$E^p_{\gamma,H}$	1.1754e-5 (α_L)	1.1455e-5 (α_O)	1.0152e-5 (α^*_O)

In order to compare the influence of different choices of grid dependent parameter α, we simulate the Darcy flow for the two cases of fractured porous media shown in Figure 5 based on DFM and EFM. We use the approximate solution obtained from the DFM (2.2) as the reference solution, and compute the errors $E^p_{m,H} = \|p^{EFM}_{m,H} - \Pi^m_H p^{DFM}_{m,h}\|_{0,\Omega_m}$ and $E^p_{\gamma,H} = \|p^{EFM}_{\gamma,H} -$

$\Pi_H^\gamma p_{\gamma,h}^{DFM}\|_{0,\gamma}$ for different choices of α. Here, Π_H^m and Π_H^γ are standard L^2-projections from the fine finite element spaces used for pressure approximation in DFM to the coarse finite element spaces used for pressure approximation in EFM. For the case of possible multiple fractures in a grid cell, we denote by α_O^* the grid dependent parameter α obtained by oversampling technique using the possible multiple fractures network in a grid cell. We still use α_L based on linear boundary condition and α_O based on oversampling technique to denote the choices of α obtained by treating each fracture in a grid cell as a single fracture. The coarse grids used for the EFM are shown in Figure 5. We test the two cases in Figure 5 with $K_m = 1, K_f = 10^6$, Dirichlet boundary condition $p_m = 1$ at $x = 0$ and $p_m = 0$ at $x = 3$, and no flow condition at $y = 0$ and $y = 3$. We can see from Table 1 that for the case of multiple fractures appearing in a grid cell, the EFM is more accurate based on α_O and α_O^* which both can be applied for real simulation. For possible complex fracture network in a grid cell, we use the EFM based on α_O^* in the following experiments.

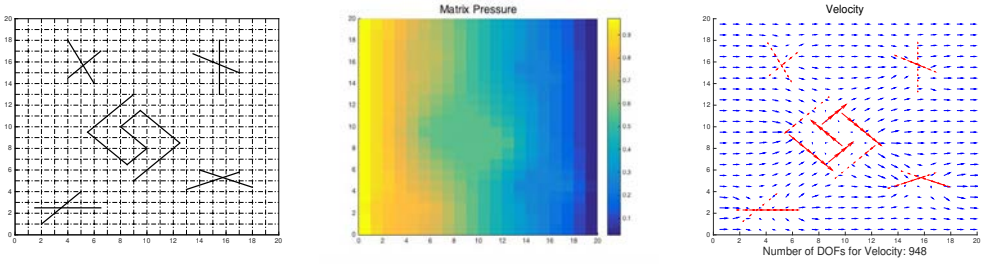

Figure 6: Left: The matrix with one dimensional fractures and the coarse grid for the EFM. Middle: Approximate pressure in matrix. Right: Approximate velocities in matrix and fractures.

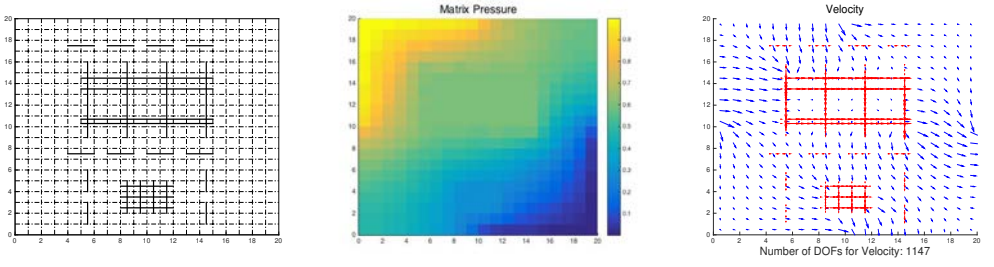

Figure 7: Left: The matrix with one dimensional fractures and the coarse grid for the EFM. Middle: Approximate pressure in matrix. Right: Approximate velocities in matrix and fractures.

Two examples based on the two-scale reduce model in the matrix domain $\Omega_m = [0, 20]^2$ are shown in Figure 6 and Figure 7. The permeabilities in matrix and fractures are assumed to be $K_m = 1$ and $K_f = 10^6$ for both two examples. In Figure 6, we test the case with Dirichlet boundary condition $p_m = 1$ at $x = 0$ and $p_m = 0$ at $x = 20$, and no flow condition at $y = 0$ and $y = 20$, while in Figure 7, we test the case with Dirichlet boundary condition $p_m = 1$ at $\{(x, y) : x = 0, y \in [10, 20]\} \cup \{(x, y) : x \in [0, 10], y = 20\}$, $p_m = 0$ at $\{(x, y) : x = 20, y \in [0, 10]\} \cup \{(x, y) : x \in [10, 20], y = 0\}$ and no flow condition at the other parts of $\partial\Omega_m$. From Figures 6-7, we can observe how the fractures influence the global pressure distribution in matrix and how the fractures collect the flow from the matrix.

5 Conclusion

The DFM and EFM, in which the fractures are dealt as a lower dimensional problems, are used in this paper to design a two-scale reduced model. The EFM is used as a coarse scale model, while the DFM is applied on the fine scale to compute an important grid dependent parameter used in the EFM. The Raviart-Thomas mixed finite element methods are utilized for the DFM on fine scale and the EFM on the coarse scale. The efficiency of the grid dependent parameter obtained by the DFM is tested. We compute two benchmark examples for the Darcy flow in fractured porous media, and make observation of the effects caused by the fractures. Future works of interest include the extension of the proposed model for the flow in the fractured porous media with anisotropic permeability in matrix and the simulation in three-dimensional fractured porous media.

References

[1] G. Barenblatt, Y. Zheltov, and I. Kochina, Basic concepts in the theory of seepage of homogeneous fluids in fissurized rocks, J. Appl. Math. Mech., 24 (1960), pp. 1286–1303.

[2] R. Baca, R. Arnett, and D. Langford, Modeling fluid flow in fractured porous rock masses by finite element techniques, Int. J. Num. Meth. Fluids, 4 (1984), pp. 337–348.

[3] F. Brezzi and M. Fortin, Mixed and Hybrid Finite Element Methods, Springer-Verlag, New York, 1991.

[4] Y. Efendiev, S. Lee, G. Li, J. Yao, and N. Zhang, Hierarchical multiscale modeling for flows in fractured media using Generalized Multiscale Finite Element Method, arXiv:1502.03828, 2015.

[5] L. Formaggia, A. Fumagalli, A. Scotti and P. Ruffo, A reduced model for Darcy's problem in networks of fractures, ESAIM Math. Model. Numer. Anal., 48 (2014), pp. 1089–1116.

[6] N. Frih, J.E. Roberts, and A. Saada, Modeling fractures as interfaces: a model for Forchheimer fractures, Comput. Geosci., 12 (2008), pp. 91–104.

[7] A. Fumagalli, Numerical Modelling of Flows in Fractured Porous Media by the XFEM Method, Ph.D. thesis, Politecnico di Milano, 2012.

[8] H. Hajibeygi, D. Karvounis, and P. Jenny, A hierarchical fracture model for the iterative multiscale finite volume method, J. Comp. Phys., 230 (2011), pp. 8729–8743.

[9] H. Hoteit and A. Firoozabadi, Multicomponent fluid flow by discontinuous Galerkin and mixed methods in unfractured and fractured media, Water Resour. Res., 41 (2005), W11412.

[10] H. Hoteit and A. Firoozabadi, An efficient numerical model for incompressible two-phase flow in fractured media, Adv. Water Resour., 31 (2008), pp. 891–905.

[11] S.H. Lee, C.L. Jensen, M.F. Lough, Efficient finite-difference model for flow in a reservoir with multiple length-scale fractures, SPE J., 3 (5) (2000), pp. 268–275.

[12] S.H. Lee, M.F. Lough, C.L. Jensen, Hierarchical modeling of flow in naturally fractured formations with multiple length scales, Water Resour. Res., 37 (2001), pp. 443–455.

[13] L. Li, S.H. Lee, Efficient field-scale simulation of black oil in naturally fractured reservoir through discrete fracture networks and homogenized media, SPE Reserv. Evaluat. Eng., (2008), pp. 750–758.

[14] V. Martin, J. Jaffré, and J.E. Roberts, Modeling fractures and barriers as interfaces for flow in porous media, SIAM J. Sci. Comput., 26 (2005), pp. 1667–1691.

[15] K. Pruess and T. Narasimhan, A practical method for modeling fluid and heat flow in fractured porous media, SPE J. 25 (1985), pp. 14–26.

[16] J. Warren, P. Root, The behavior of naturally fractured reservoirs, SPE J., 1963, pp. 245–255.